Malaysian Journal of Energy and Applications 1 (2026): 57-70
https://doi.org/10.17576/myjea.2026.01.57

QUATERNIZED POLY(VINYL ALCOHOL)/QUATERNIZED GRAPHENE OXIDE COMPOSITE MEMBRANES: IMPACT OF FILLER LOADING ON PERFORMANCE

Kiranraj Vaiyanan Kannan[1], Ramanidevi Balachandran[2], Wai Yin Wong[1] &
Mohd Shahbudin Mastar @ Masdar[1,2]*

[1] *Fuel Cell Institute, Universiti Kebangsaan Malaysia, 43600 UKM Bangi, Selangor.*
[2] *Faculty of Engineering & Built Environment, Universiti Kebangsaan Malaysia.*

**Corresponding author email: shahbud@ukm.edu.my*

Received 1/7/2026; Received in Revised Form 13/7/2026;
Accepted 13/7/2026; Available Online 20/07/2026.

Abstract

As global efforts accelerate toward deep decarbonisation, anion exchange membrane (AEM) water electrolysis offers a versatile, zero-emission pathway to generate green hydrogen for heavy industries, grids, and hydrogen fuel cells. Pristine polyvinyl alcohol has lower conductivity and ion exchange capacity compared to quaternized polyvinyl alcohol (QPVA) due to low cationic region. Hence, QPVA faces several challenges such as lower ionic conductivity compared to commercial AEM standards, poor alkaline stability, excessive KOH uptake that causes over swelling and lower durability (membrane becomes soft). These challenges can be mitigated by studying the parameters of polymer modifications by studying implementing of nanofillers with different weight percentage ratio of quaternized graphene oxide (QGO) filler to improve ionic conductivity, improve mechanical properties of membrane while reducing excessive swelling and with degree of crosslinking can reduce overswell while improving mechanical strength. Here, composite AEMs based on quaternized poly(vinyl alcohol) (QPVA) and quaternized graphene oxide (QGO) were fabricated via doctor blade casting to evaluate the effect of QGO loading (0.5, 1.0, and 2.0 wt.%). FTIR, XRD, and FESEM-EDX confirmed successful functionalization, revealing a homogeneous filler dispersion at 1.0 wt.% but particle agglomeration at 2.0 wt.%. QGO inclusion directly modulated the dynamic viscosity, surface tension, and water contact angle of the casting solutions. Upon transitioning from 5.0 M KOH activation to 1.0 M KOH equilibration, the optimized 1.0 wt.% membrane minimized thickness swelling to 4.88% while achieving a peak ionic conductivity of 10.79 mS/cm due to its uniform microstructural pathways. Conversely, the over-loaded 2.0 wt.% sample uniquely exhibited simultaneous increases in swelling (8.29% to 8.92%) and conductivity (2.95 to 4.47 mS/cm) as water pooled within agglomeration-induced micro voids. Overall, these findings demonstrate that optimizing QGO loading to 1.0 wt.% via controlled doctor blade casting yields structurally stable composite AEMs suitable for its exploration in efficient green hydrogen generation.

Keywords: QPVA polymer matrix; QPVA/QGO composite membrane; Anion exchange membrane; green hydrogen; renewable fuel source

1.0 Introduction

Anion exchange membrane (AEM) water electrolysis has emerged as a compelling green hydrogen production technology, merging the low operational costs of alkaline water electrolysis (AWE) with the high power density of proton exchange membrane (PEM) systems

[1].Beyond its primary application in powering clean hydrogen fuel cells, the high-purity green hydrogen produced via this method serves as a versatile, low-carbon energy carrier, facilitating deep decarbonization within heavy industries and enhancing the stability of renewable energy grids. By utilizing non-noble metal electrocatalysts and polymer-based membranes functionalized with quaternary ammonium cationic groups, AEM systems significantly lower capital costs while maintaining efficient ion transport [2]. However, AEM water electrolysis still faces operational setbacks during system operation that can reduce overall electrolyzer efficiency and hydrogen output [3]. In these setups, ion transport is heavily influenced by variables such as ionic conductivity, hydration levels, and membrane stability, where the AEM serves as the primary ion-conducting medium and electrical insulator [4].

The widespread application of AEMs is frequently hindered by low ionic conductivity, primarily attributed to slow hydroxide ion transport kinetics and low dissociation rates [4]. Consequently, structural and compositional modifications, such as the incorporation of inorganic fillers [5] and the optimization of membrane thickness, are essential to dictate the overall efficiency of the composite system [6-8].While not yet widely adopted as a standard industry material, polyvinyl alcohol (PVA)-based membranes have been explored as an affordable alternative for AEMs due to their cost-effectiveness, flexible polymer backbone modification, and chemical resistance. However, maintaining high operational efficiency remains a significant challenge; pristine PVA membranes often exhibit low ionic conductivity and excessive water uptake that compromises their structural integrity, leading to accelerated chemical degradation via Hofmann elimination or S_N2 pathways [9, 10].

To counteract these limitations, the introduction of quaternary ammonium (QA) groups into PVA via modification with glycidyltrimethylammonium chloride (GTMAC) yields quaternized polyvinyl alcohol (QPVA), which significantly enhances both ionic conductivity and mechanical stability [11].The electrochemical performance of these matrices can be further enhanced through the incorporation of inorganic fillers like graphene oxide (GO), where the interactions between QA groups and the oxygen-containing functional groups of GO improve the chemical, thermal, and mechanical stability of the composite membrane while creating hydrophilic domains that facilitate efficient ion transport [12]. Although GO-based membranes have shown improved ionic conductivity. Hence, in previous study Z, Zakaria et al. [11] only mentioned using QPVA/GO for ethanol-based fuel cell. Thus, functionalizing GO with quaternary ammonium groups using a dimethyloctadecyl [3-(trimethoxysilyl)propyl] ammonium chloride (DMAOP) precursor to produce quaternized graphene oxide (QGO) can enhance cationic region on QGO surface, in which increases as anion exchange capability and able to tune QPVA/QGO for AEM fuel cell and water electrolyser. [11, 13]. Beyond chemical composition, the fabrication technique is important, conventional solution casting shows moderate thickness control with uniformity at larger scale. In contrast, the doctor blade technique offers a robust, scalable alternative with superior thickness control and film consistency with even disperse on polymer solution and nanofillers throughout membrane surfaces [14].

Currently, a significant research gap exists regarding how the concurrent utilization of doctor blade casting as alternative casting method, PVA quaternization, and QGO filler incorporation that enhance anion exchange capability on membrane surfaces in which can be tailored to simultaneously optimize film uniformity, hydrolytic stability, and ionic conductivity. To address this gap, the objective of this study is to systematically synthesize and characterize QPVA/QGO composite membranes fabricated via the doctor blade technique at a targeted 50 µm baseline thickness across varying QGO loadings (0.5, 1.0, and 2.0 wt.%). The rheological and physicochemical properties of the QPVA/QGO solutions such as viscosity, surface tension, and contact angle are evaluated alongside membrane structural

characterizations (FESEM-EDX, FTIR, and XRD) to observe the resulting improvements in membrane homogeneity and electrochemical performance.

2.0 Experimental

2.1 Preparation of QPVA solution

Polyvinyl alcohol (PVA) was obtained from Sigma-Aldrich (molecular weight, M_w: 85,000–124,000 g/mol, 99+% hydrolysed). To prepare the base solution, PVA crystals (7 wt.%) were dissolved in deionized (DI) water and stirred under heating until dissolved. The temperature was subsequently reduced to 65 °C, and stirring was continued until the solution became completely transparent. To perform the quaternization at a targeted 2:2:1 molar ratio (GTMAC:KOH:PVA), glycidyltrimethylammonium chloride (GTMAC, Sigma–Aldrich, ≥90% technical grade, calculated based on dry substance) and a 2 M potassium hydroxide (KOH) solution were added to the PVA solution. The resulting mixture was stirred for 4 h at 75 °C. Subsequently, absolute ethanol (Merck, 99.9%) was slowly added to the mixture to precipitate the quaternized PVA (QPVA). The collected precipitate was isolated and dried in a vacuum oven overnight at 60 °C. Finally, the dried QPVA precipitate was redissolved in DI water under continuous stirring to yield the final QPVA solution [15].

2.2 Preparation of cross-linked QPVA/QGO composite membrane

To prepare the 0.5 wt.% quaternized graphene oxide (QGO) filler solution, QGO powder was sonicated in small quantity of DI water until fully dispersed. This step was replicated using to produce the 1.0 wt.% and 2.0 wt.% QGO solutions, respectively. The 0.5 wt.% QGO solution was subsequently mixed with 90 mL of the QPVA solution and sonicated until a completely homogeneous QPVA/QGO casting solution was obtained; this blending procedure was repeated identically for the 1.0 wt.% and 2.0 wt.% QGO variants.

For membrane fabrication, 30 mL of each QPVA/QGO mixture was cast using a doctor blade at a controlled thickness of 50 µm. The cast films were allowed to air-dry on the apparatus until they could be safely peeled off, followed by overnight drying in a vacuum oven at 60 °C. The membranes were then thermally cured in a vacuum oven for 3 h at 80 °C and an additional 1 h at 100 °C. Afterward, the membranes were cut into standardized 2.7 cm × 2.7 cm samples for testing. Chemical cross-linking was carried out by immersing the membranes in a 10 vol.% glutaraldehyde solution (Grade II, 25% in H_2O) prepared in acetone (Merck) for 2 h at room temperature (RT). Finally, the membranes were activated in a 5 M KOH solution for 24 h at 60 °C, followed by equilibration in a 1 M KOH solution for 24 h at room temperature.

2.3 Characterization of QPVA/QGO membranes

2.3.1 Physicochemical Characterizations

Fourier transform infrared (FTIR) spectra of the membrane samples were recorded using a Spectrum 400 FT-IR/NIR Imaging System (PerkinElmer). The spectra of the dried membrane samples were acquired in the wavenumber range of 4000 to 400 cm^{-1} at a resolution of 4 cm^{-1} over 32 scans. X-ray diffraction (XRD) patterns of the samples were obtained using a D8

Advance diffractometer (Bruker) equipped with Cu Kα radiation (1.5406 Å) operated at 40 kV and 40 mA. The scanning 2θ range was set from 5° to 80°, and the collected data were analysed using HighScore Plus software. The surface morphology of the membrane samples was observed via field emission scanning electron microscopy (FESEM) using a MERLIN microscope (ZEISS). All samples were completely dried and sputter-coated with gold prior to measurement. The surface elemental composition of the samples was evaluated using energy-dispersive X-ray spectroscopy (EDX). The dynamic viscosity of the prepared QPVA and QPVA/QGO polymer casting solutions was evaluated at room temperature using a Brookfield DV2T digital rotational viscometer. Measurements were recorded across a range of rotational speeds (5, 10, and 25 rpm) to analyse the rheological behaviour and shear-thinning characteristics of the solutions prior to membrane casting.

2.3.2 Swelling ratio and ionic conductivity

The dry thickness of the QPVA/QGO membranes (t_{dry}) was measured using a micrometer gauge after cross-linking. The corresponding hydrated thickness (t_{wet}) was recorded after the membranes were activated in the KOH solution. The thickness swelling ratio (SR) was then calculated using equation (1):

$$Swelling\ ratio = \frac{t_{wet-} - t_{dry}}{t_{dry}} \quad (1)$$

The ionic conductivity of the QPVA and QPVA/QGO composite membranes was evaluated at room temperature using a standard two-electrode cell configuration connected to an electrochemical workstation (Autolab PGSTAT M204). The membranes were evaluated after immersion in 5 M and 1 M KOH solutions. The bulk membrane resistance (R_s) was determined from the intercept on the real axis of the Nyquist plot, analysed using Nova software. The ionic conductivity (λ) was calculated using equation (2):

$$\lambda = \frac{t}{A \times R_S} \quad (2)$$

where t is membrane thickness (cm), A is the active area of the membrane (cm^2) and R_S is the measured membrane resistance (Ω).

3. Results and discussion

3.1 Chemical and Structural Characterization

Fourier transform infrared (FTIR) analysis was conducted to identify the functional groups present within the QPVA/QGO composite membrane samples. Figure 1 displays the FTIR spectra of the fabricated QPVA/QGO composite membranes. Spectral analysis reveals a noticeable reduction in the intensity of aliphatic C–H bending vibrations following the quaternization and cross-linking of the QPVA/QGO membranes. Compared to pristine QPVA, several new characteristic peaks emerged. Specifically, the peak at 1330 cm^{-1} is attributed to aliphatic C–N stretching, signifying the successful integration of quaternary ammonium groups into the polymer backbone [11]. Furthermore, the prominent absorption band at approximately 1093 cm^{-1} corresponds to C–O–C stretching, which confirms the cross-linking network facilitated by glutaraldehyde (GA) [16]. The presence of peaks at 918 cm^{-1} (epoxy C–O symmetric stretching) and 1413 cm^{-1} (carboxylic O=C–O stretching) further validates the successful incorporation of the QGO component [13]. The appearance of a peak at 1656 cm^{-1} is attributed to C=C stretching within the aromatic structure of QGO, reflecting its hydrophobic domains and their interaction with the QPVA matrix backbone [13, 16]. Additionally, the broad and intense absorption band at 3288 cm^{-1} corresponds to hydroxyl (–OH) stretching vibrations.

Overall, these spectra confirm the existence of functional groups consistent with literature reports, thereby validating the successful synthesis of cross-linked QPVA/QGO composite membranes.

To evaluate how these chemical modifications altered the internal physical architecture of the polymer matrix, X-ray diffraction (XRD) analysis was performed. Figure 2 illustrates the XRD patterns of the QPVA and QPVA/QGO composite membranes across the scanning 2θ range of 5° to 80°. The pristine QPVA membrane exhibits a characteristic prominent crystalline reflection peak at 2θ around 19.5°, corresponding to the semi-crystalline backbone structure of PVA. Upon the incorporation of QGO fillers (0.5, 1.0, and 2.0 wt.%), a slight decrease in the intensity of this primary PVA reflection peak is observed, indicating that the introduction of functionalized QGO nanosheets disrupts the intermolecular hydrogen bonding and close chain packing within the matrix. Furthermore, the peak identified at 2θ = 28.06° is attributed to QGO, reflecting the presence of partially stacked or restacked graphene layers [17]. The low intensity of this peak indicates a highly homogeneous dispersion of QGO within the QPVA matrix, confirming the successful integration of the nanofiller across all composite membranes [11]. The corresponding crystallinity percentages calculated from these diffraction profiles are detailed in Table 1.

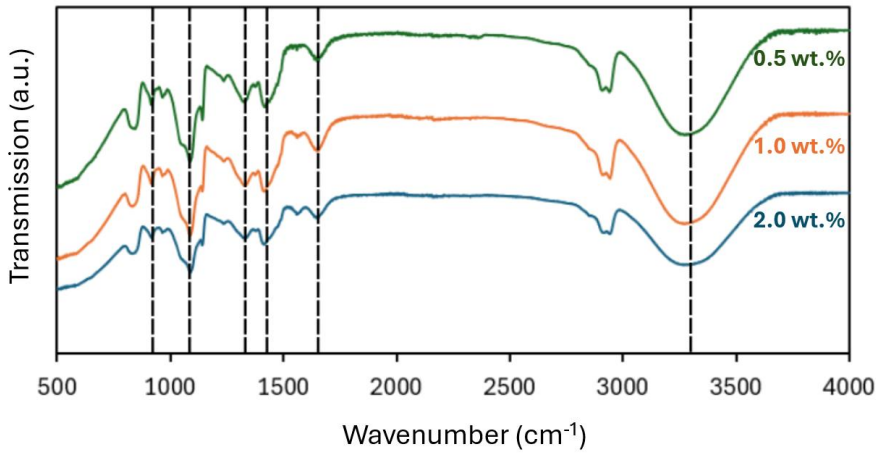

Figure 1: FTIR spectra of QPVA/QGO composite membranes at various QGO filler loadings (0.5 wt.%, 1.0 wt.%, and 2.0 wt.%).

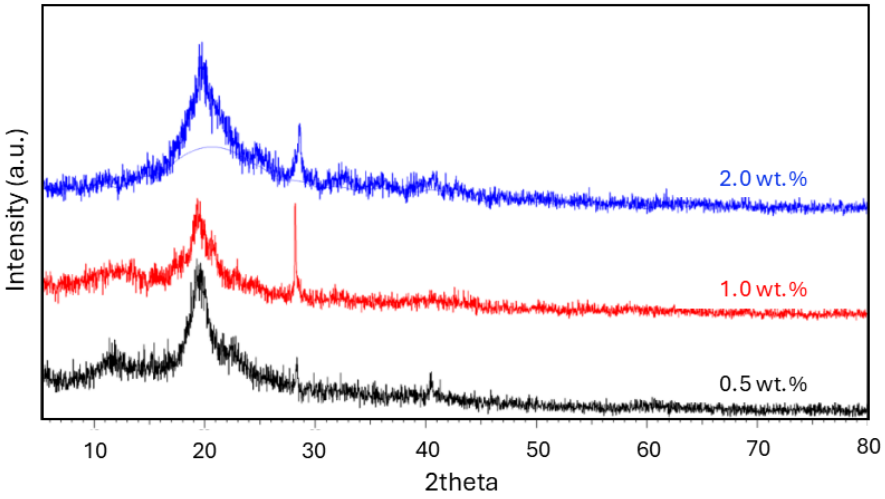

Figure 2: XRD spectra of QPVA/QGO composite membranes at various QGO filler loadings (0.5 wt.%, 1.0 wt.%, and 2.0 wt.%).

Table 1: Calculated crystallinity percentages for QPVA/QGO composite membranes as a function of QGO content.

Membranes	Crystallinity percentage (%)
QPVA/QGO$_{0.5\ wt.\%}$	45.3
QPVA/QGO$_{1.0\ wt.\%}$	31.9
QPVA/QGO$_{2.0\ wt.\%}$	25.8

3.2 Rheological Properties and Surface Properties of the Casting Solutions

The rheological properties of pristine QPVA and QPVA/QGO solutions were evaluated at QGO concentrations of 0.5, 1.0, and 2.0 wt.%. Figure 3 illustrates the dynamic viscosity profiles and rheological behaviour of the QPVA/QGO casting solutions under varying rotational speeds (5, 10, and 25 rpm) as a function of QGO content.

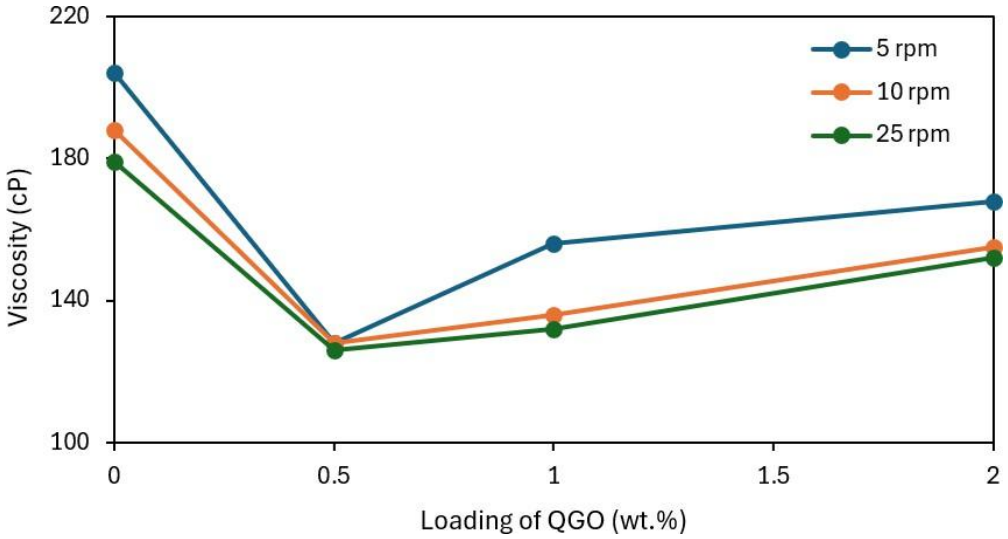

Figure 3: Dynamic viscosity profiles of pristine QPVA and QPVA/QGO composite casting solutions as a function of QGO filler loading under varying rotational speeds (5, 10, and 25 rpm).

Because both the pristine QPVA matrix and the QGO fillers carry positive charges, they exhibit strong electrostatic repulsion at the molecular level. At a low filler concentration of 0.5 wt.%, the highly dispersed QGO nanosheets act as physical barriers that restrict polymer chain entanglement. Consequently, the QPVA chains minimize their interaction with the charged fillers, leading to a reduction in hydrodynamic volume and a subsequent decrease in fluid resistance [18]. This phenomenon induces the formation of highly localized, low-friction shearing planes, resulting in a precipitous reduction in macro-viscosity compared to pristine QPVA. However, increasing the QGO concentration to 1.0 wt.% and 2.0 wt.% occupies the available free volume within the polymer matrix, driving the composite solution into a critical crowding threshold. Despite the persistent electrostatic repulsion between the QPVA chains and QGO fillers, the high packing density significantly restricts molecular mobility, which shifts the viscosity upward [19, 20]. Across all samples, the viscosity decreases as the rotational speed increases from 5 to 25 rpm, demonstrating characteristic non-Newtonian, shear-thinning (pseudoplastic) behaviour. Controlling this solution viscosity is crucial for the doctor blade casting method, as the shear forces applied during the sliding motion of the blade dictate the uniformity of the film and prevent uneven dispersion.

To complement the rheological evaluation, an analysis of the surface tension and contact angle was conducted for the QPVA/QGO solutions with varying QGO loadings. The resulting data are summarized in Table 3, while Figure 4 illustrates the droplet morphology and corresponding contact angles for each loading condition.

Table 3: Surface tension and water contact angle of QPVA/QGO composite casting solutions

QGO loading(wt.%)	Surface tension (mN/m)	Contact angle (°)
0.5	72.33±1.33	40.51±0.32
1.0	66.84±0.93	52.66±1.27
2.0	65.90±0.34	32.69±0.37

As shown by the contact angle trends in Figure 4, the 1.0 wt.% QGO loading yielded the highest contact angle 52.66° compared to the 0.5 wt.% and 2.0 wt.% concentrations, indicating a localized minimum in surface hydrophilicity [21]. Generally, increased QGO loading introduces a higher surface concentration of mobile quaternary ammonium groups, which typically enhances hydrophilicity and drives down the contact angle, as observed in the sharp decrease to32.69° at 2.0 wt.%. However, the 1.0 wt.% threshold represents an anomalous optimal loading point where the QGO is perfectly and uniformly dispersed within the polymer matrix, as corroborated by subsequent FESEM observations. In contrast, the 0.5 wt.% loading exhibited a lower contact angle (40.51°) despite possessing a higher surface tension (72.33 mN/m), which is likely due to insufficient filler coverage that leaves patches of the base QPVA matrix exposed [22]. These findings suggest that surface roughness, interfacial energy, and filler dispersion quality are the primary determinants of the membrane's wetting behaviour. Ultimately, the surface tension, contact angle, and viscosity play a collective role during doctor blade casting, as they govern the cohesion of the polymer solution and its wetting interactions with the casting substrate (such as glass or PET) to ensure defect-free membranes.

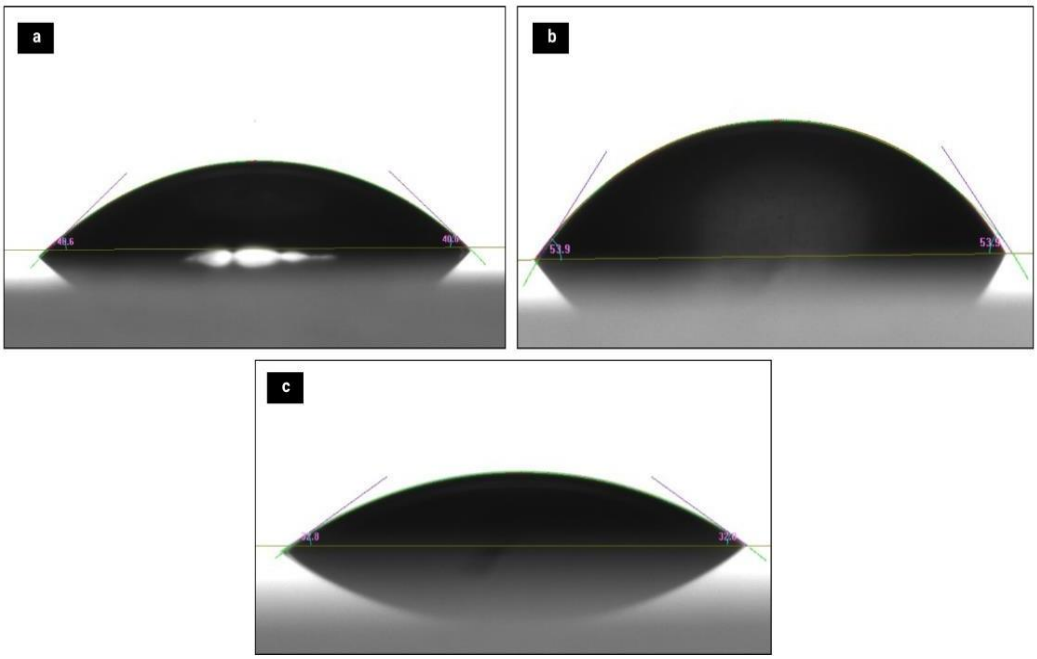

Figure 4: Water contact angle profiles and droplet shapes of QPVA/QGO composite membranes with 0.5 wt.%, 1.0 wt.%, and 2.0 wt.% QGO loadings.

3.3 Morphological and Elemental Analysis

The surface morphology and elemental composition of the QPVA/QGO membranes were characterized using field emission scanning electron microscopy (FESEM) coupled with energy-dispersive X-ray spectroscopy (EDX). This analysis provided a comprehensive assessment of the surface topology and elemental distribution across the designated membrane areas. FESEM micrographs captured at 1000× magnification, alongside the corresponding EDX mappings for all samples, are presented in Figure 5.

Based on Figures 5a–c (most right panels), the membrane surface contrast darkens as the filler loading within the polymer matrix increases. Furthermore, based on table 5 shows QPVA/QGO composite membranes yield controlled thickness between 47 – 49 µm. The QPVA/QGO membrane integrated with 1.0 wt.% QGO displays a highly uniform morphology, indicating a homogeneous dispersion of the nanofiller within the polymer matrix (Figure 5e). In contrast, increasing the QGO loading to 2.0 wt.% results in observable filler agglomeration (Figure 5f). This high weight percentage compromises dispersion quality, leading to an excessive filler density that obstructs the ion transport pathways of the host QPVA polymer [11, 23].

EDX mapping of the QPVA/QGO composite membranes identifies the constituent elements as carbon (C), oxygen (O), potassium (K), and chlorine (Cl). Visual analysis confirms a uniform elemental distribution throughout the composite matrix, with carbon emerging as the dominant element. Notably, the relative oxygen content within the matrix increases in direct correlation with the higher wt.% filler loading due to the oxygen-rich functional groups on the QGO. Concurrently, a substantial reduction in the relative chlorine elemental composition is observed, dropping from 15.7% to 0.6%. This reduction is primarily attributed to the increased concentration of QGO per unit area, suggesting that the dense network and structural interactions within the QPVA/QGO matrix effectively displace or dilute the chlorine content within the scanned framework. Ultimately, FESEM and EDX mapping provide a comprehensive characterization of the morphology, packing density, and elemental distribution within the composite structure, with detailed values summarized in Table 4.

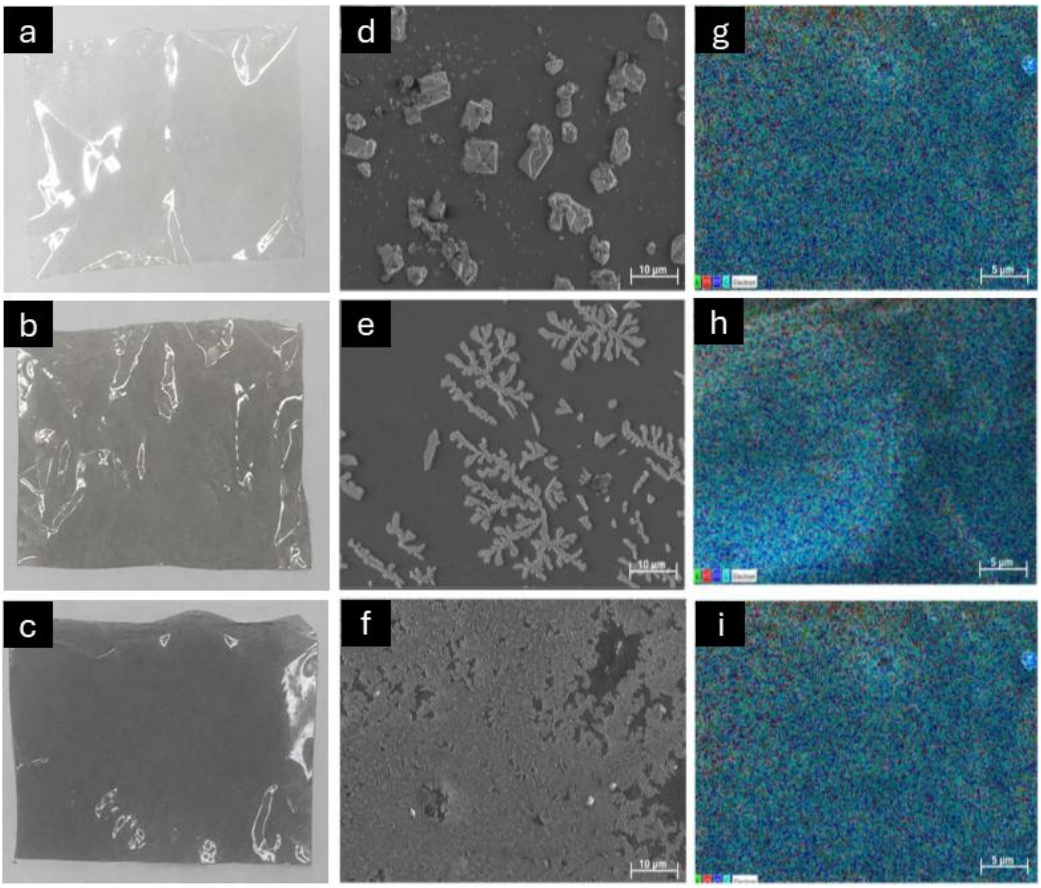

Figure 5: (a – c) Raw image of QPVA/QGO membranes, (d – f) FESEM morphology and (g – i) EDX mapping of the membranes with QGO wt.% loading of 0.5 wt.%, 1.0 wt.% & 2.0 wt.% respectively

Table 4: Elemental compositions of QPVA/QGO membrane

	Composition of Elements (%)		
Elements	**QPVA/QGO$_{0.5\ wt.\%}$**	**QPVA/QGO$_{1.0\ wt.\%}$**	**QPVA/QGO$_{2.0\ wt.\%}$**
Carbon	55.3	67.7	68.4
Oxygen	12.7	28.4	29.6
Potassium	16.3	2.4	1.4
Chlorine	15.7	1.5	0.6

3.4 Swelling Ratio and Ion Conductivity

Table 5 demonstrates that the incorporation of QGO fillers and subsequent alkaline treatment conditions exert a profound dual influence on the dimensional stability and electrochemical properties of the fabricated AEMs. A distinct and contrasting trend in both thickness swelling and ionic conductivity is observed when comparing the membranes immediately after activation in a highly concentrated 5.0 M KOH solution versus after equilibration in a lower-concentration 1.0 M KOH solution.

Table 5: Swelling ratio and ion conductivity

Membranes	Dry thickness(μm)	Activation of membranes in 5M KOH		Equilibration of membranes in 1M KOH	
		Thickness swelling (%)	Ion conductivity (mS/cm)	Thickness swelling (%)	Ion conductivity (mS/cm)
QPVA	49.22± 3.60	23.75±4.96	4.09±0.30	11.25±1.40	4.69 ±0.56
QPVA/QGO$_{0.5}$ wt.%	48.56 ± 7.27	11.50 ± 4.42	5.45 ± 0.99	8.19 ± 4.14	5.60 ± 0.55
QPVA/QGO$_{1.0}$ wt.%	48.33 ± 2.52	41.46 ± 4.29	7.74 ± 1.65	4.88 ± 3.82	10.79 ± 3.32
QPVA/QGO$_{2.0}$ wt.%	47.11 ± 1.92	8.29 ± 2.25	2.95 ± 0.60	8.92± 6.44	4.47±0.46

During the initial activation phase in 5.0 M KOH, the QPVA/QGO 1.0 wt.% membrane exhibits an exceptionally high thickness swelling ratio of 41.46%, which is accompanied by an ionic conductivity of 7.74 mS/cm. This significant spike in swelling is dictated by thermodynamic and osmotic phenomena. Because the 1.0 wt.% loading provides an optimal and highly uniform distribution of quaternary ammonium functional groups across both the QPVA matrix and the QGO nanosheets, it creates a high density of accessible hydrophilic ionic domains. When immersed in a highly concentrated 5.0 M KOH solution, an immense osmotic pressure gradient is generated between the external electrolyte and the membrane interior, drawing a massive influx of OH^- and K^+ ions into these domains. This intense ion crowding triggers severe electrostatic repulsion among the closely packed ions within the hydrophilic channels, forcing the polymer chains to stretch extensively and resulting in a severe swelling profile. In sharp contrast, when the 1.0 wt.% membrane is subsequently transferred and allowed to equilibrate in a milder 1.0 M KOH environment, a dramatic structural recovery occurs. The thickness swelling ratio plummets to a minimum of 4.88%, while its ionic conductivity simultaneously surges to a peak value of 10.79 mS/cm. This behavioural shift aligns with the principles established by Zakaria et al. [11], demonstrating that optimal filler loading can successfully modulate swelling and maximize conductivity under standardized operational conditions. The mechanism behind this improvement during 1.0 M KOH equilibration can be explained by structural deswelling and channel optimization, as illustrated by the structural relationship between hydration and ion hopping.

When the external alkaline concentration drops from 5.0 M to 1.0 M, the severe internal osmotic pressure is relieved, causing excess unbound free-alkali ions to diffuse out of the membrane. This concentration reduction allows the elastic contractile forces of the glutaraldehyde (GA) cross-linked polymer network to reassert control, pulling the expanded matrix back into a structurally stabilized, low-swelling state (4.88%). Crucially, this moderate hydration state works in perfect synergy with the membrane's microstructural architecture. As established in the FESEM analysis (Section 3.3), the 1.0 wt.% QGO composite exhibits a highly homogeneous morphology, characterized by a uniform distribution of the functionalized nanofiller throughout the host polymer matrix. This structural consistency ensures that during matrix contraction upon equilibration, the continuous network of interconnected hydrophilic pathways remains intact without collapsing or fragmenting. Free from the severe

macrostructural tortuosity and phase separation that typically hinders ion migration, the localized quaternary ammonium sites achieve an optimized spatial arrangement. Instead, the well-dispersed QGO nanosheets remain perfectly aligned to form continuous, uninterrupted ionic highways across the membrane profile. This allows the hydroxide (OH^-) ions to migrate with improved efficiency, driving the conductivity up to its peak value of 10.79 mS/cm.

A highly intriguing and reversed trend is observed for the over-loaded 2.0 wt.% QGO composite membrane, where both thickness swelling and ionic conductivity increase when moving from 5.0 M KOH to 1.0 M KOH. In the highly concentrated 5.0 M KOH activation solution, the extreme ionic strength of the external environment creates a hypertonic osmotic effect that essentially dehydrates the membrane. Because the 2.0 wt.% sample suffers from severe nanoparticle agglomeration, its polymer network is highly phase-separated and rigid, restricting water uptake to just 8.29%. This lack of internal water molecules deprives the system of the hydration required for ion transport, resulting in a severely restricted baseline conductivity of 2.95 mS/cm. However, when transferred to the lower-concentration 1.0 M KOH solution, the external osmotic pressure drops significantly, allowing water to readily penetrate the membrane matrix. For this over-loaded sample, the accumulated water molecules pool inside the loose interfacial micro voids and cracks caused by the QGO agglomerates [24, 25]. This hydration influx causes the thickness swelling to rise from 8.29% to 8.92%. Crucially, this additional water presence helps re-hydrate the remaining functional pathways and facilitates greater liquid-phase ion mobility, which explains the corresponding rise in ionic conductivity from 2.95 mS/cm to 4.47 mS/cm.

Despite this localized improvement, the conductivity of the 2.0 wt.% membrane remains drastically lower than that of the optimized 1.0 wt.% sample (10.79 mS/cm) because the agglomerated clusters permanently block continuous, long-range anion transport channels. Ultimately, a comparative analysis across both chemical environments confirms that the 1.0 wt.% QGO loading represents a definitive performance threshold. This configuration leverages the transition between activation and equilibration to yield improved dimensional stability and peak electrochemical performance, as visually summarized by the direct correlation plotted in Figure 6.

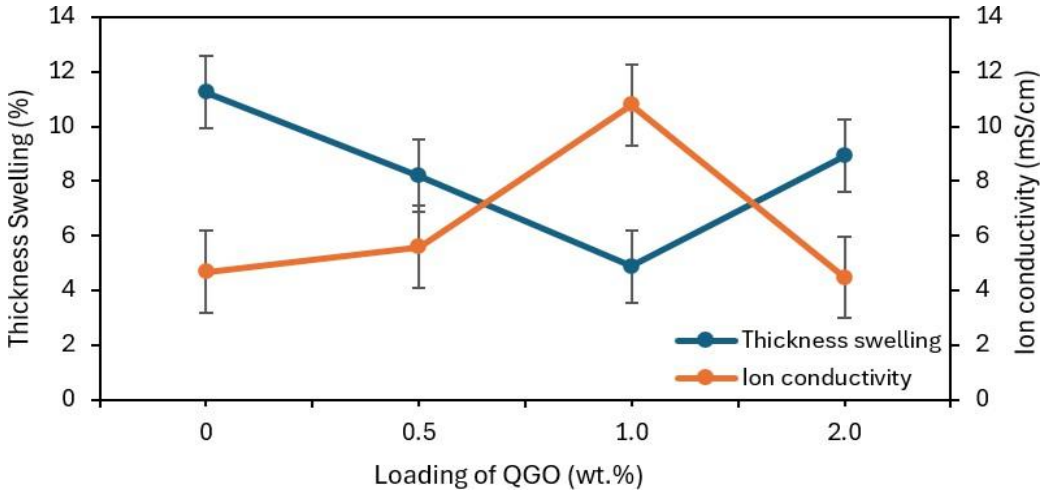

Figure 6: Graph of swelling ratio and ion conductivity at 1 M KOH against QGO loading

Conclusion

In conclusion, this study successfully fabricated uniform quaternized polyvinyl alcohol and quaternized graphene oxide (QPVA/QGO) composite membranes utilizing the doctor blade casting technique for anion exchange membrane water electrolysis. Characterization via FTIR, XRD, and FESEM-EDX confirmed successful chemical functionalization and revealed that a 1.0 wt.% QGO loading yields a homogeneous filler dispersion, whereas a higher loading of 2.0 wt.% induces particle agglomeration. Dimensional and electrochemical evaluations proved that the 1.0 wt.% QGO concentration represents the optimal loading point, achieving a minimized thickness swelling of 4.88% and a peak ionic conductivity of 10.79 mS/cm after equilibration in 1.0 M KOH. Overall, this work demonstrates that the combination of polymer quaternization, optimized nanofiller loading, and controlled doctor blade casting offers a viable approach to producing structurally stable composite membranes for efficient green hydrogen production.

Acknowledgment

The authors gratefully acknowledge the financial support provided by the Ministry of Higher Education Malaysia through the Higher Education Centre of Excellence (HICoE) Program awarded to the Fuel Cell Institute, Universiti Kebangsaan Malaysia (Grant No. HICOE-2023-004).

Author Contributions

The authors declare that they contributed equally to all stages of this manuscript and research.

Declaration of Competing Interest

The authors declare that they have no known competing financial interests or personal relationships that could have appeared to influence the work reported in this paper.

Declaration of Generative AI and AI-Assisted Technologies in the Writing Process

During the preparation of this manuscript, the authors utilized Gemini Pro AI strictly for grammatical editing, proofreading, and language enhancement to improve text readability. The AI assistance was limited to refining sentence structures and phrasing, with no role in experimental data generation, data analysis, or the formulation of scientific conclusions. The authors have thoroughly reviewed and verified the final text and accept full responsibility for the accuracy, integrity, and authenticity of the content presented in this work.

References

1. Vincent, I., E.-C. Lee, and H.-M. Kim, *Comprehensive impedance investigation of low-cost anion exchange membrane electrolysis for large-scale hydrogen production.* Scientific Reports, 2021. **11**(1): p. 293.

2. Liu, L., et al., *Recent Advances and Challenges in Anion Exchange Membranes Development/Application for Water Electrolysis: A Review.* Membranes (Basel), 2024. **14**(4).
3. Noor Azam, A.M.I., et al., *Investigation of Performance of Anion Exchange Membrane (AEM) Electrolysis with Different Operating Conditions.* Polymers (Basel), 2023. **15**(5).
4. Samsudin, A.M., M. Bodner, and V. Hacker, *A Brief Review of Poly(Vinyl Alcohol)-Based Anion Exchange Membranes for Alkaline Fuel Cells.* Polymers (Basel), 2022. **14**(17).
5. Zakaria, Z. and S.K. Kamarudin, *A review of quaternized polyvinyl alcohol as an alternative polymeric membrane in DMFCs and DEFCs.* International Journal of Energy Research, 2020. **44**: p. 6223 - 6239.
6. Samsudin, A.M., et al., *Preparation and Characterization of QPVA/PDDA Electrospun Nanofiber Anion Exchange Membranes for Alkaline Fuel Cells.* Nanomaterials (Basel), 2022. **12**(22).
7. Zakaria, Z. and S.K. Kamarudin, *Evaluation of Quaternized polyvinyl alcohol/graphene oxide-based membrane towards improving the performance of air-breathing passive direct methanol fuel cells.* International Journal of Energy Research, 2020. **44**(11): p. 8988-9000.
8. Samsudin, A.M. and V. Hacker, *Effect of Crosslinking on the Properties of QPVA/PDDA Anion Exchange Membranes for Fuel Cells Application.* Journal of The Electrochemical Society, 2021. **168**(4).
9. Dennis, J.O., et al., *A Review of Current Trends on Polyvinyl Alcohol (PVA)-Based Solid Polymer Electrolytes.* Molecules, 2023. **28**(4).
10. Choudhury, R.R., J.M. Gohil, and K. Dutta, *Poly(vinyl alcohol)-based membranes for fuel cell and water treatment applications: A review on recent advancements.* Polymers for Advanced Technologies, 2021. **32**(11): p. 4175-4203.
11. Zakaria, Z., S.K. Kamarudin, and S.N. Timmiati, *Influence of Graphene Oxide on the Ethanol Permeability and Ionic Conductivity of QPVA-Based Membrane in Passive Alkaline Direct Ethanol Fuel Cells.* Nanoscale Res Lett, 2019. **14**(1): p. 28.
12. Kleut, D. and J. Prekodravac Filipovic, *Advances in Graphene Oxide-Based Composites and Membranes: Structural Engineering, Multifunctional Performance, and Emerging Applications.* Processes, 2025. **14**(1).
13. Zarrin, H., et al., *Quaternized Graphene Oxide Nanocomposites as Fast Hydroxide Conductors.* ACS Nano, 2015. **9**(2): p. 2028-2037.
14. Dyartanti, E.R., et al., *Recent Development of Polyvinylidene Fluoride/Cellulose Membranes Electrolyte Separator for Lithium Ion Batteries.* IOP Conference Series: Materials Science and Engineering, 2021. **1096**(1): p. 012144.
15. Ng, W.K., et al., *The impact of double crosslinking and alkaline activation strategies on the multifaceted characteristics of quaternized poly(vinyl alcohol) anion exchange membranes.* Energy Advances, 2025. **4**(3): p. 400-413.
16. Shaari, N., S.K. Kamarudin, and Z. Zakaria, *Enhanced alkaline stability and performance of alkali-doped quaternized poly(vinyl alcohol) membranes for passive direct ethanol fuel cell.* International Journal of Energy Research, 2019. **43**(10): p. 5252-5265.
17. Gupta, B., et al., *Role of oxygen functional groups in reduced graphene oxide for lubrication.* Sci Rep, 2017. **7**: p. 45030.
18. Kopac, T., A. Rucigaj, and M. Krajnc, *Effect of polymer-polymer interactions on the flow behavior of some polysaccharide-based hydrogel blends.* Carbohydr Polym, 2022. **287**: p. 119352.
19. Ghannam, M.T., et al., *Viscosity Characteristics of Cationic Polyacrylamide Aqueous Solutions.* Polymers (Basel), 2026. **18**(3).

20. Hu, J., et al., *Main Controlling Factors Affecting the Viscosity of Polymer Solution due to the Influence of Polymerized Cations in High-Salt Oilfield Wastewater.* Processes, 2024. **12**(4).
21. Brack, H., *A contact angle investigation of the surface properties of selected proton-conducting radiation-grafted membranes.* Journal of Membrane Science, 2003. **214**(1): p. 1-19.
22. Zhang, Q., et al., *Structural and Transport Properties of Hydrophilic and Hydrophobic Modified Ionomers in Proton Exchange Membrane Fuel Cells.* Polymers (Basel), 2024. **16**(5).
23. Kumar, S.R., et al., *Synergistic role of graphene oxide-magnetite nanofillers contribution on ionic conductivity and permeability for polybenzimidazole membrane electrolytes.* Journal of Power Sources, 2020. **445**.
24. Hasan, M.R. and J. Coronas, *How Can the Filler-Polymer Interaction in Mixed Matrix Membranes Be Enhanced?* Chempluschem, 2024. **89**(12): p. e202400456.
25. Sardarabadi, H., et al., *Effect of Nanofillers on Properties and Pervaporation Performance of Nanocomposite Membranes: A Review.* Membranes (Basel), 2022. **12**(12).